

1 Long-term real-time chemical characterization of submicron aerosols
2 at Montsec (Southern Pyrenees, 1570 m a.s.l.)

3
4 A. Ripoll^{1,2*}, M. C. Minguillón¹, J. Pey³, J. L. Jimenez⁴, D. A. Day⁴, Y.
5 Sosedova⁵, F. Canonaco⁵, A. S. H. Prévôt⁵, X. Querol¹, and A. Alastuey¹

6 ¹Institute of Environmental Assessment and Water Research (IDAEA-CSIC),
7 Jordi Girona 18-26, 08034, Barcelona, Spain

8 ² Department of Astronomy and Meteorology, Faculty of Physics, University of
9 Barcelona, Martí i Franquès 1, 08028, Barcelona, Spain

10 ³Aix-Marseille Université, CNRS, LCE FRE 3416, Marseille, 13331, France

11 ⁴Department of Chemistry and Biochemistry, and Cooperative Institute for
12 Research in the Environmental Sciences (CIRES), University of Colorado at Boulder,
13 80309, CO, USA

14 ⁵Paul Scherrer Institute, Laboratory of Atmospheric Chemistry, 5232 Villigen
15 PSI, Switzerland

16 *Correspondence to: A. Ripoll (anna.ripoll@idaea.csic.es)

17

18 **Abstract.** Real-time measurements of inorganic (sulfate, nitrate, ammonium,
19 chloride and black carbon (BC)) and organic submicron aerosols (aerosols with an
20 aerodynamic diameter less than 1 μm) from a continental background site (Montsec,
21 MSC, 1570 m a.s.l.) in the Western Mediterranean Basin (WMB) were conducted for 10
22 months (July 2011 - April 2012). An Aerosol Chemical Speciation Monitor (ACSM) was
23 co-located with other on-line and off-line PM_{10} measurements. Analyses of the hourly,
24 diurnal, and seasonal variations are presented here, for the first time for this region.

25 Seasonal trends in PM_{10} components are attributed to variations in: evolution of
26 the planetary boundary layer (PBL) height, air mass origin, and meteorological
27 conditions. In summer, the higher temperature and solar radiation increases
28 convection, enhancing the growth of the PBL and the transport of anthropogenic
29 pollutants towards high altitude sites. Furthermore, the regional recirculation of air
30 masses over the WMB creates a continuous increase in the background concentrations
31 of PM_{10} components and causes the formation of reservoir layers at relatively high
32 altitudes. The combination of all these atmospheric processes results in a high
33 variability of PM_{10} components, with poorly defined daily patterns, except for the organic
34 aerosols (OA). OA was mostly composed (up to 90%) of oxygenated organic aerosol
35 (OOA), split in two types: semi-volatile (SV-OOA) and low-volatile (LV-OOA), the rest
36 being hydrocarbon-like OA (HOA). The marked diurnal cycles of OA components
37 regardless of the air mass origin indicates that they are not only associated with
38 anthropogenic and long-range-transported secondary OA (SOA), but also with recently-
39 produced biogenic SOA.

40 Very different conditions drive the aerosol phenomenology in winter at MSC.
41 The thermal inversions and the lower vertical development of the PBL leave MSC in
42 the free troposphere most of the day, being affected by PBL air masses only after
43 midday, when the mountain breezes transport emissions from the adjacent valleys and
44 plains to the top of the mountain. This results in clear diurnal patterns of both organic
45 and inorganic concentrations. OA was also mainly composed (71%) of OOA, with
46 contributions from HOA (5%) and biomass burning OA (BBOA; 24%). Moreover, in
47 winter sporadic long-range transport from mainland Europe is observed.

48 The results obtained in the present study highlight the importance of SOA
49 formation processes at a remote site such as MSC, especially in summer. Additional
50 research is needed to characterize the sources and processes of SOA formation at
51 remote sites.

52

53 **Keywords:** high altitude, mountain, remote, continental background, ACSM.

54

55 1 Introduction

56 Earth's climate system is modulated by atmospheric aerosols. Submicron
57 particles ($< 1 \mu\text{m}$ in aerodynamic diameter) play a dominant role in both cloud
58 formation and scattering or absorbing solar radiation (IPCC, 2013). The complexity of
59 aerosol sources and processes results in an uncertainty in the radiative forcing of
60 climate. Aerosol optical properties are connected to direct and indirect climate forcing
61 effects, and they are dependent on particle composition. Moreover, aerosol
62 composition may provide valuable information on aerosol sources and processes.
63 Consequently, long-term measurements of PM_{10} chemical composition are needed to
64 better understand aerosol sources, to quantify their lifetime in the atmosphere and to
65 constrain the uncertainties of their climatic influence.

66 Long-term PM_{10} chemical composition measurements are relatively scarce both
67 off-line and on-line. In the last decade, on-line PM_{10} chemical composition
68 measurements have been performed using aerosol mass spectrometers (AMS) at a
69 number of locations. Measurements of on-line chemical composition are useful to study
70 hourly variations and daily patterns. Most of these studies, however, correspond to
71 short-term measurement campaigns (typically a month) (e.g. Crippa et al., 2014;
72 Jimenez et al., 2009; Lanz et al., 2010; Ng et al., 2010; Zhang et al., 2007) given the
73 intensive instrument maintenance required and the need of highly-qualified personnel
74 for a good quality dataset.

75 In contrast to the use of the AMS in relatively short campaigns, the more
76 recently developed Aerodyne Aerosol Chemical Speciation Monitor (ACSM) is
77 becoming a widely used on-line instrument for long-term measurements of PM_{10}
78 chemical composition (Budisulistiorini et al., 2014; Canonaco et al., 2013; Petit et al.,
79 2014; Tiitta et al., 2014). The ACSM is built upon the same technology as the AMS, in
80 which an aerodynamic particle focusing lens is combined with high vacuum thermal
81 particle vaporization, electron impact ionization, and mass spectrometry. Modifications
82 in the ACSM design (e.g. lack of particle sizing chamber and components, use of
83 simple and compact RGA mass spectrometer detector), however, allow it to be smaller,
84 lower cost, and simpler to operate than the AMS (Ng et al., 2011c). The ACTRIS
85 (Aerosols, Clouds, and Trace gases Research InfraStructure) European network is
86 evaluating the use of the ACSM as a reliable instrument, which will provide the
87 opportunity to study long-term datasets of PM_{10} chemical composition across the
88 continent.

89 Recent publications have investigated most of the existing worldwide AMS
90 databases (e.g. Crippa et al., 2014; Jimenez et al., 2009; Lanz et al., 2010; Ng et al.,
91 2010; Zhang et al., 2007) and reflected a prevalence of organic aerosols (20 to 90%) in

92 the submicron fraction, largely independent of the region and type of environment.
93 However, our knowledge on organic aerosol (OA) formation, sources, and atmospheric
94 processing is still very incomplete, especially for secondary organic aerosols (SOA)
95 formed from chemical reactions of gas-phase species (e. g. Donahue et al., 2014;
96 Hallquist et al., 2009; Kroll and Seinfeld, 2008; Robinson et al., 2007; Volkamer et al.,
97 2006). Recent progress has been made in identifying primary organic aerosols (POA)
98 sources (e.g. Elbert et al., 2007; Zhang et al., 2005), but significant gaps still remain in
99 our understanding on the atmospheric evolution of POA after emission (de Gouw and
100 Jimenez, 2009). For these reasons, OA measurements and analysis are required to
101 better understand its chemical evolution in the atmosphere.

102 The lack of long-term on-line PM_1 chemical composition measurements is
103 especially evident in the Western Mediterranean Basin (WMB), which is characterized
104 by particular atmospheric dynamics strongly influenced by its topography (Jorba et al.,
105 2013; Millan et al., 1997). Over this region, arrival of natural and anthropogenic
106 aerosols as a result of long-range transport from Africa and Europe is frequent (e.g.
107 Pey et al., 2013; Querol et al., 2009; Ripoll et al., 2014; Rodríguez et al., 2001) and
108 accumulation and recirculation processes are frequently observed (Rodríguez et al.,
109 2002). The sources and meteorological controls of PM in the regional background of
110 the WMB have been recently investigated during the DAURE study (Pandolfi et al.,
111 2014a) using an AMS and ^{14}C analyses (Crippa et al., 2014; Minguillón et al., 2011).
112 Furthermore, Ripoll et al. (2015) studied the PM_1 and PM_{10} chemical composition with
113 daily time resolution in the continental and regional background environments in the
114 WMB. In that study, a higher mineral contribution was identified in the continental
115 background due to the preferential transport of African dust at high altitude layers and
116 to the increased regional dust resuspension enhanced by the drier surface and higher
117 convection. Nevertheless, aerosol chemical characterization with higher time resolution
118 is needed to study the origin of specific PM components and the local and/or regional
119 processes, in particular to exploit the information contained in diurnal cycles that is
120 typically not accessible with off-line measurements.

121 In this study we deployed an ACSM at a high altitude site (Montsec, 1570 m
122 a.s.l.) in the NE of the Iberian Peninsula ($42^\circ 03' N$, $0^\circ 44' E$), representative of the
123 continental background conditions of the Western Mediterranean Basin (WMB) (Ripoll
124 et al., 2014). This environment is under free tropospheric (FT) influence most of the
125 time, although it is exposed to regional pollutants during the summer time and/or under
126 the influence of mountain breezes, and it is affected by trans-boundary incursions of
127 natural and anthropogenic aerosols from Europe and North Africa (Ripoll et al., 2014,
128 2015). Co-located on-line and off-line PM_1 measurements were also carried out to

129 complement the ACSM dataset. Hence, the work presented here interprets the real-
130 time variation of inorganic and organic submicron components during 10 months (July
131 2011 - April 2012), and the types of OA are also studied. Special emphasis is placed
132 on the analysis of diurnal pattern and seasonal variations of chemical components and
133 the main factors influencing these variations.

134 **2 Methodology**

135 *2.1 Sampling site*

136 Montsec site (MSC) is located on the highest part of the Montsec d'Ares
137 mountain, at an altitude of 1570 m a.s.l., in a plain near the edge of a 1000 m cliff to the
138 south, with no wind obstructions present around. It is located in the NE of the Iberian
139 Peninsula (42°03'N, 0°43'E), 50 km S of the Pyrenees and 140 km NW of Barcelona
140 (Fig.S1). A detailed description of this site can be found in Ripoll et al. (2014). This
141 station is a member of the GAW (global atmospheric watch) network as a regional
142 station named MSA.

143 The daily classification of atmospheric episodes affecting MSC was made
144 following the procedure described by Ripoll et al. (2014) using HYSPLIT model from
145 the NOAA Air Resources Laboratory (ARL). Air masses reaching MSC are mainly from
146 the Atlantic (62% of the days) all along the year. From March to October, North African
147 (NAF) episodes are more frequent (17% of the days) and very often are alternated with
148 the summer regional (SREG) scenarios (12% of the days). The winter regional
149 (WREG) scenarios are detected from October to March (11% of the days), as well as
150 the European (EU) episodes (11% of the days). Conversely, the Mediterranean (MED)
151 episodes are detected sporadically (4% of the days).

152 The boundary layer height was calculated using the Global Data Assimilation
153 System (GDAS1) model from the NOAA Air Resources Laboratory
154 (<http://www.ready.noaa.gov/READYamet.php>) (Fig. 1).

155 *2.2 ACSM sampling and data analysis*

156 The aerosol chemical speciation monitor (ACSM) (Aerodyne Research Inc.)
157 was measuring continuously from July 2011 to April 2012. The ACSM provides real-
158 time mass concentration of submicron particulate organics, nitrate, sulfate, ammonium
159 and chloride via thermal vaporization and electron impact ionization, with detection by a
160 quadrupole mass spectrometer (Ng et al., 2011c). The mass concentration of a given
161 species is determined from the sum of the ion signals at each of its mass spectral
162 fragments and its Ionization Efficiency (IE) (Canagaratna et al., 2007). Since calibration
163 of IEs for all species is not feasible, the Relative Ionization Efficiency (RIE) (compared

164 to that of nitrate) is used (Jimenez et al., 2003). The ammonium nitrate calibration
165 described by Ng et al. (2011b) was performed using an atomizer (TSI, Constant Output
166 Atomizer model 3076) for primary aerosol generation, followed by a silica gel diffusion
167 dryer, a differential mobility analyzer (DMA) model TSI [3081](#), and a condensation
168 particle counter (CPC, TSI 3772). Monodisperse 300 nm ammonium nitrate aerosol
169 particles were used, covering a range of nitrate concentrations from 2 to 15 $\mu\text{g m}^{-3}$.
170 Several calibrations were conducted throughout the sampling period, and average
171 values of 2.2×10^{-11} for nitrate IE and 5.4 for RIE for ammonium were used for the
172 whole dataset. The RIE values used in this study for the rest of the species were those
173 usually applied in AMS ambient concentrations: 1.4 for OA and 1.1, 1.2, and 1.3 for
174 nitrate, sulfate, and chloride, respectively (Canagaratna et al., 2007). RIE for sulfate
175 was experimentally determined one year later and was found to be 1.26, although the
176 default value was used for the current dataset. A time resolution of 62 minutes was
177 used as a result of 12 scans (1 open and 1 filtered) per data point with a scan speed of
178 1 s amu^{-1} .

179 The ACSM data were analyzed with the standard ACSM data analysis software
180 version 1.5.3.2 (Aerodyne Research Inc.) written in Igor Pro 6 (WaveMetrics, Inc., Lake
181 Oswego, OR, USA). As the ACSM was measuring continuously for a long time, the
182 standard correction for instrument sensitivity drifts was applied to the dataset based on
183 the inlet pressure and N_2 signal. Finally, mass concentrations were corrected using a
184 Collection Efficiency (CE) to account for the particle bounce of aerosols on the
185 vaporizer. The composition-dependent CE was calculated as described by Middlebrook
186 et al. (2012) and was close to 0.45 for most of the time. Since for most ambient studies
187 a 0.5 CE value is found to be representative with data uncertainties generally within
188 $\pm 20\%$ (Canagaratna et al., 2007), and since our ACSM concentrations using CE=0.5
189 were in good agreement with concentrations from other co-located instruments, a CE
190 of 0.5 was used.

191 The organic components were further investigated by applying Multilinear
192 Engine (ME-2) (Paatero, 1999) to the organic mass spectra. With the ME-2, the user
193 can introduce a priori information about sources with the so-called a-value approach.
194 Hence, the user inputs one or more factor profiles and a constraint defined by the a-
195 value, which determines the extent to which the output profile can differ from the profile
196 fed to the model. The source apportionment of OA was performed applying ME-2 using
197 the custom software tool of Source Finder (SoFi) version 4.8 developed by Canonaco
198 et al. (2013). The ME-2 analysis was carried out separately for the summer period (14
199 Jul 11 – 24 Sep 11) and the winter period (10 Jan 12 – 7 Mar 12). Only $m/z \leq 100$ were
200 used for source apportionment of OA because: a) the signals of $m/z > 100$ account for a

201 minor fraction of the total organic mass (on average, 2 %), b) the $m/z > 100$ have larger
202 uncertainties, and c) the large interference of naphthalene signals (used for m/z
203 calibration of the ACSM) at these m/z (e.g., m/z 127, 128, and 129) (Sun et al., 2012).

204 2.3 Co-located measurements used in this study

205 MSC has been permanently equipped with aerosol monitoring instrumentation
206 since January 2010 and some of these measurements were used in this study. The 24
207 h PM_{10} samples were collected every 4 days on 150 mm quartz micro-fiber filters
208 (Pallflex QAT) using high volume samplers ($30 \text{ m}^3 \text{ h}^{-1}$, MCV CAV-A/MSb) equipped
209 with MCV PM_{10} cut-off inlets. Daily PM_{10} mass concentrations were determined by off-
210 line gravimetric procedures according to the EN 12341 standard (CEN, 1999), i.e. at
211 20°C temperature and 50% relative humidity. Furthermore, PM_{10} chemical composition
212 was obtained as described by Ripoll et al. (2015) using inductively coupled plasma
213 atomic emission spectroscopy (ICP-AES) and mass spectrometry (ICP-MS) for major
214 and trace elements, respectively, ion high performance liquid chromatography (HPLC)
215 and selective electrode for ions concentrations, and thermal-optical method (using the
216 EUSSAR 2 protocol) for elemental carbon (EC) and organic carbon (OC)
217 concentrations. Real-time PM_{10} mass concentrations were continuously measured by an
218 optical particle counter (OPC, model GRIMM 1.107 calibrated with different latex PSL
219 refraction index 1.59). PM_{10} 30-minute data were daily averaged and subsequently
220 corrected by comparison with 24 h standard gravimetric mass measurements. The
221 absorption coefficient was measured continuously at 637 nm using a multi-angle
222 absorption photometer (MAAP, model 5012, Thermo). Equivalent black carbon (BC)
223 mass concentrations (Petzold et al., 2013) were calculated by the MAAP instrument
224 software by dividing the measured absorption coefficient $\sigma_{ap}(\lambda)$ by $6.6 \text{ m}^2 \text{ g}^{-1}$, which is
225 the instrument default mass absorption cross section (MAC) at 637 nm (Müller et al.,
226 2011; Petzold and Schönlinner, 2004). Particle scattering (σ_{sp} ; $0^\circ - 360^\circ$) and
227 hemispheric backscattering (σ_{bsp} ; $90^\circ - 270^\circ$) coefficients at three wavelengths (450nm,
228 525nm, 635nm) were measured with a LED-based integrating nephelometer (model
229 Aurora 3000, ECOTECH Pty, Ltd, Knoxfield, Australia).

230 Finally, all meteorological data were measured by the Catalanian
231 Meteorological Service from the Montsec d'Ares station. Gaseous pollutants (O_3 , NO,
232 NO_2 , CO and SO_2) were measured using real-time monitors belonging to the Network
233 of Control and Surveillance of Air Quality of the Autonomous Government of Catalonia.
234 NO and NO_2 concentrations were measured using a Thermo Scientific instrument,
235 model 42i-TL; CO using a Teledyne 300 EU Gas filter correlation analyzer; O_3 using a

236 MCV 48AV UV photometry analyzer; and SO₂ using a Teledyne 100 EU UV
237 fluorescence analyzer.

238 In addition to these routine measurements, 2 intensive campaigns were
239 performed in July - August 2011 and January - February 2012. During these intensive
240 campaigns PM₁ filters were collected daily and a scanning mobility particle sizer
241 (SMPS) was installed to measure particle number size distribution of mobility diameters
242 11-350 nm in the summer campaign, and 8-450 nm in the winter campaign. The SMPS
243 system comprises a classifier unit (model TSI 3080) and a differential mobility analyzer
244 (DMA, model TSI 3081) connected to a condensation particle counter (CPC, model TSI
245 3772). The SMPS data for the winter campaign were also used to estimate the mass
246 concentration to compare with the ACSM data. To this end, the volume size
247 distributions were calculated from the measured particle number distributions assuming
248 sphericity. The total volume concentrations were computed by integrating over the
249 measured particle range and converted to mass concentration using the estimated
250 composition-dependent density, calculated using the chemical composition given by
251 the ACSM and the equation of Salcedo et al. (2006). Average concentrations shown in
252 the whole paper are arithmetic averages unless otherwise specified.

253 **3 Results and discussion**

254 *3.1 Submicron aerosol mass concentrations*

255 In order to establish the consistency of the different measurements during this
256 study, the sum of the ACSM species (= sulfate + nitrate + ammonium + OA + chloride)
257 and the BC mass concentrations was compared with the co-located PM₁ and light
258 scattering measurements (Fig. 2). The scatter plots of ACSM plus BC concentrations
259 versus PM₁ concentrations from the OPC and SMPS showed strong correlations
260 ($R^2=0.72$ and $R^2=0.87$, respectively) and slopes close to unity (slope=0.94 and
261 intercept=0.09 for the ACSM+BC vs. OPC, and slope=1.21 and intercept=0.86 for the
262 ACSM+BC vs. SMPS) (**¡Error! No se encuentra el origen de la referencia.**). The
263 differences in the particle size range measured by the different instruments needs to be
264 considered when assessing these comparisons. Moreover, ACSM plus BC
265 concentrations were also highly correlated with light scattering at 525 nm determined
266 by the nephelometer ($R^2=0.85$, **¡Error! No se encuentra el origen de la referencia.**).
267 The high degree of agreement is also apparent in the time series plots of PM₁ shown in
268 Fig. 2.

269 The average concentration (25th, 50th, 75th percentiles) of the ACSM + BC mass during
270 during this study (July 2011 - April 2012) was 4.9 $\mu\text{g m}^{-3}$ (0.9, 2.8, 7.9 $\mu\text{g m}^{-3}$) (

271 Table 1), which is similar to the 2010-2012 average reported by Ripoll et al. (2014)
272 from OPC measurements ($5.0 \mu\text{g m}^{-3}$). For the sake of brevity only summer (14 Jul 11
273 – 24 Sep 11) and winter (10 Jan 12 – 7 Mar 12) hourly variation will be discussed in the
274 following sections, given that hourly variation in spring was similar to summer and that
275 in fall was similar to winter. The seasonal average PM_{10} concentrations were higher in
276 summer ($7.5 \mu\text{g m}^{-3}$) (3.4, 7.1, $10.5 \mu\text{g m}^{-3}$),

277 Table 1) than in winter ($4.1 \mu\text{g m}^{-3}$ (0.8, 1.7, $5.6 \mu\text{g m}^{-3}$),

278 Table 1). A similar seasonal pattern has been described at other high altitude
279 sites in Europe (e.g. Carbone et al., 2014; Cozic et al., 2008; Freney et al., 2011; Tositti
280 et al., 2013), being associated with differences in the air mass origin from summer to
281 winter, and also to variations in the planetary boundary layer (PBL) height. The
282 seasonal variation at MSC has been described in detail in recent works (Pandolfi et al.,
283 2014b; Ripoll et al., 2014, 2015), and it has been principally attributed to the seasonal
284 variation of the PBL (Fig. 1). In summer, the stable anticyclonic conditions over this
285 continental area enhance convection increasing the development of the PBL and
286 favoring the transport of anthropogenic pollutants towards high altitude sites such as
287 MSC. The situation in winter is notably different, as the lower vertical development of
288 the PBL over this area leaves high altitude sites in the FT, isolating MSC from polluted
289 air masses. The seasonal variation of PM concentrations at MSC has been also
290 connected to mesoscale and synoptic processes. At MSC, southern flows and regional
291 recirculation episodes are more frequent in summer, whereas clean Atlantic advections
292 and northeastern winds from mainland Europe are more common in winter (Fig.S2 and
293 Table S1) (Pandolfi et al., 2014b; Ripoll et al., 2014, 2015). Moreover, the summer
294 maximum has been ascribed to the more vigorous photochemistry in the atmosphere
295 that enhances the formation of secondary inorganic and organic aerosols (Querol et al.,
296 1999).

297 3.2 Submicron aerosol chemical composition

298 Concentrations of ACSM species were daily averaged and compared with off-
299 line measurements from 24-h PM₁ samples, and all species showed strong correlations
300 (R^2 between 0.77 and 0.96, Fig.S3). Different slopes (ACSM vs off-line measurements)
301 were found for each of the species: 1.12 for sulfate, 1.31 for ammonium and 1.35 for
302 nitrate. The relatively higher slope for nitrate, with respect to sulfate, could be attributed
303 to a sampling negative artifact due to the volatilization of nitrate on the off-line samples
304 (Schaap et al., 2004). Ammonium is present as a counterion for sulfate and nitrate, and
305 thus its slope is in between those of the two species.

306 The OM-to-OC ratio can not be determined for ACSMs based on f44 following
307 Aiken et al. (2008) as concluded from an intercomparison of 13 ACSMs (Fröhlich et al.,
308 2015). Therefore, the OM-to-OC in the present study was estimated from the slope of
309 OA, measured by ACSM, vs. OC, obtained from off-line measurements. This slope was
310 found to be 3.39, however values of 2.2 are more common for aged aerosol (e.g. Aiken
311 et al., 2008; Minguillón et al., 2011; Takahama et al., 2011). This disagreement of a
312 factor of 1.54 may be attributed to different reasons. A negative volatilization artifact
313 may occur in the filters, hence resulting in an underestimation of OC. Alternatively it is

314 possible that the RIE for OA in the ACSM is larger than the value of 1.4 determined for
315 the AMS, a topic currently being investigated by the ACSM manufacturer, which would
316 result in an overestimation of OA. Similar series of intercomparisons with a similar
317 discrepancy for OA has been found for a one-year dataset (June 2012 – July 2013)
318 with the same instrument at Montseny site (Minguillón et al., 2015) and for a recently
319 reported study in Atlanta, US by Budisulistiorini et al. (2014). Assuming that the
320 disagreement was due to the overestimation by the ACSM, the OA concentrations
321 were corrected dividing by the disagreement factor (1.54) to compare the results with
322 co-located measurements (**Error! No se encuentra el origen de la referencia.**). The
323 resulting slopes were very similar and hence OA concentrations reported in the present
324 paper were not corrected since further research is needed to better estimate the RIE
325 for OA in the ACSM.

326 The average of PM₁ chemical composition at MSC during this study (July 2011 - April
327 April 2012) is given in Fig. 4. On average, OA was the largest PM₁ constituent (50%),
328 followed by sulfate (20%), nitrate (14%), ammonium (12%), BC (4%) and chloride (1%).
329 As was the case of PM₁ concentrations, all chemical components increased in summer
330 and decreased in winter, with the exception of nitrate (Fig. 4 and

331 Table 1). The higher nitrate concentrations in winter than in summer were also
332 observed in other studies in the Mediterranean region (e.g. Pey et al., 2009; Querol et
333 al., 2009; Ripoll et al., 2015) and this variation was attributed to the high volatility of
334 ammonium nitrate at low humidity and high temperature (Zhuang et al., 1999). At MSC,
335 the summer maximum of the rest of PM components has been mainly ascribed to the
336 higher temperature and solar radiation in summer (Table S1), which enhances
337 atmospheric photochemistry, promoting the formation of secondary inorganic and
338 organic aerosols. All these seasonal characteristics are described in detail in Ripoll et
339 al. (2015).

340 3.2.1 Summer trends

341 Time series of PM₁ components during summer time (14 Jul – 24 Sep 2011) are
342 shown in Fig. 5. Wind direction and wind speed, temperature, precipitation and
343 concentrations of nitrogen oxides, sulfur dioxide, and ozone are also depicted. The
344 daily classification of atmospheric episodes affecting MSC is also illustrated in different
345 background colors. On average, during summer the lowest concentrations of all PM₁
346 components and gases were recorded under the Atlantic advection conditions since
347 these air masses are associated with precipitation, decreased temperature and solar
348 radiation, and strong winds, leading to cleaner atmospheric conditions. Conversely,
349 summer regional episodes lasted for 6 to 11 consecutive days and led to sustained
350 increases of the background concentrations of sulfate, OA and BC at MSC. Despite the
351 limited ACSM data availability during North African episodes, relatively high
352 concentrations of PM₁ components were observed under this type of episodes,
353 especially BC (Fig. 5).

354 The diurnal cycles of PM₁ components, gaseous pollutants and meteorological
355 variables are shown in Fig. 6. The summer concentrations of PM₁ components and
356 gases showed no clear diurnal patterns, except for ozone and OA. This lack of defined
357 daily patterns is similar to the findings obtained at the high altitude Puy-de-Dôme
358 station in central France (Freney et al., 2011, the only similar study found at a remote
359 site). For a high altitude site as MSC, the lack of diurnal cycles can be explained by a
360 combination of factors. In summer, the recirculation of air masses over the WMB
361 induced by an abrupt orography (Fig.S1) causes the formation of reservoir layers at
362 any time at relatively high altitudes (Millan et al., 1997; Rodríguez et al., 2003).
363 Moreover, long-range transport from North Africa, which can be more intense at high
364 altitude layers (Ripoll et al., 2015), could also blur the daily patterns since the
365 occurrence of this transport does not depend on the time of the day. These factors
366 result in a lack of well-defined daily patterns but in a high variability of diurnal cycles

367 even within the same type of episode, which is reflected in the similar average daily
368 evolutions and the high standard deviations calculated for the average daily patterns
369 when separated by air mass origin (Fig.S4).

370 The ozone and OA concentrations had a marked diurnal cycle regardless of the
371 air mass origin (Fig. 6 and Fig.S4) in summer. These different daily patterns with
372 respect to the rest of the gases and chemical components points to the fact that ozone
373 and OA variations are strongly influenced by local/regional processes and not just
374 dominated by long-range transport. Minimum ozone concentrations were recorded
375 between 8:00 and 9:00 UTC (Coordinated Universal Time, which is local time - 1:00h
376 and local summer time - 2:00h), whereas maximum concentrations were measured
377 between 16:00 and 17:00 UTC. In contrast, the highest OA concentrations were
378 observed around 12:00 UTC, and the lowest during the night and in the early morning.
379 The ozone variations may influence those of OA, although the complete understanding
380 of the ozone diurnal evolution is outside the scope of this study. The average increase
381 in OA during the day is likely due to the photooxidation of volatile organic compounds
382 (VOCs). Given that MSC is a remote site, in summer VOCs are most likely dominated
383 by local biogenic emissions (BVOCs), as it was found in the Mediterranean forested
384 area of Montseny (Seco et al., 2011). Hence, the midday increase is likely due to
385 recently-produced biogenic SOA, and to a lesser degree, photooxidation of
386 anthropogenic VOCs.

387 Despite the marked diurnal cycle of OA regardless of air mass origin, the
388 average increase during the day with respect to average concentrations during the
389 night was higher under summer regional ($2.6 \mu\text{g m}^{-3}$) and North African ($3.0 \mu\text{g m}^{-3}$)
390 episodes than during Atlantic advections ($1.3 \mu\text{g m}^{-3}$) (Fig.S4). This difference could be
391 caused by the higher SOA formation. This is due to the increase in BVOCs emissions
392 and atmospheric photooxidation caused by the higher temperature and solar radiation
393 (Paasonen et al., 2013; Seco et al., 2011) under summer regional and North African
394 episodes. Furthermore, under these episodes higher concentrations of ozone were
395 measured, which also favors the formation of SOA (via direct oxidation and also by
396 leading to higher OH concentrations). The SOA formation registered at MSC is
397 relatively high when compared to other high altitude sites such as Puy-de-Dôme
398 (Freney et al., 2011). This is in agreement with the modeled SOA emissions over
399 Europe, which identified higher SOA concentrations in Mediterranean environments
400 (Bessagnet et al., 2008). This higher SOA formation is probably due to the higher
401 emissions of BVOCs in the Mediterranean forested areas (up to 3 times higher than
402 Boreal forested areas) (Bessagnet et al., 2008; Lang-Yona et al., 2010; Steinbrecher et
403 al., 2009) and the comparable concentrations of tropospheric ozone with other high

404 altitude European sites (Chevalier et al., 2007). On the other hand, the extra formation
405 of SOA under summer regional and North African episodes might also have a
406 contribution from the photooxidation of anthropogenic VOCs, since Atlantic advections
407 are associated with cleaner atmospheric conditions.

408 3.2.2 Winter trends

409 Similar to summer, the lowest concentrations of all PM₁ components and gases
410 in winter (10 Jan 12 – 7 Mar 12) were recorded under the Atlantic advections, whereas
411 the highest were measured when MSC was affected by air masses from mainland
412 Europe and sporadically under regional conditions (Fig. 7). Mediterranean air masses
413 were detected very infrequently and therefore conclusions on their characteristics will
414 not be drawn in the present paper. The relative contribution of different components
415 was similar, with OA representing a somewhat smaller fraction than in summer.

416 In contrast to what was found in summer, in winter concentrations of most PM₁
417 components and gaseous pollutants showed much clearer diurnal patterns, with a
418 minimum around 7:00 UTC and a maximum between 14:00 and 15:00 UTC (Fig. 6).
419 Similar patterns have been observed at the Puy-de-Dôme station during a winter
420 campaign (Freney et al., 2011). These daily cycles are probably caused by the fact that
421 MSC is located most of the day within the FT in winter, whereas PBL air masses are
422 only injected upwards after midday (Fig. 1). Moreover, thermal inversions are very
423 frequent from 20:00 to 07:00 UTC. These situations prevent the transport of pollutants
424 from the lower populated areas towards higher altitudes, especially at night. During the
425 morning, the thermal inversions dissipate due to the radiative warming of the ground
426 and mountain upslope winds develop (e.g. Henne et al., 2004). These mountain winds
427 transport anthropogenic emissions from the adjacent valleys and plains to the top of
428 the mountain, with a maximum upslope transport in the afternoon. Moreover, biogenic
429 emissions influence cannot be ruled out as average winter temperatures are high
430 enough for them to occur (Seco et al., 2011; Steinbrecher et al., 2009). Thus, mountain
431 breezes play an important role in determining the diurnal variation of PM₁ components
432 in winter (Fig. 6), especially under regional conditions. A clear example of the PM₁
433 components diurnal pattern under winter regional episodes was observed from 22 to 25
434 February 2012 with PM₁ concentrations (and NO_x) increasing several fold during the
435 afternoon (Fig. 7).

436 The study of the daily cycles as a function of air mass origin (Fig.S5) showed
437 clear diurnal patterns under winter regional episodes, as mentioned above, and less
438 marked daily patterns when MSC is affected by Atlantic advections and long-range
439 transport from mainland Europe. Under Atlantic episodes the concentrations of PM₁

440 components were very low and the standard deviations with respect to the average
441 pattern were quite high, resulting in unclear diurnal patterns compared to those under
442 winter regional conditions. During European episodes, which can be more intense at
443 high altitude layers (Ripoll et al., 2015; Sicard et al., 2011), background concentrations
444 of PM₁ components were higher and the midday increment was lower compared to
445 those under winter regional conditions, resulting in less marked daily patterns. These
446 less-marked diurnal cycles are probably due to the fact that the increase of PM₁
447 components occurs during these episodes regardless of the time of the day. A good
448 example of this less-marked diurnal variation during European episodes was observed
449 from 17 to 19 February 2012 (Fig. 7).

450 3.3 Characterization of OA components

451 In order to better characterize the profiles of OA components, the ME-2 analysis
452 was performed separately for the summer period (14 Jul – 24 Sep 2011) and the winter
453 period (10 Jan 12 – 7 Mar 12), since OA components are expected to vary throughout
454 the year. The solution of ME-2 analysis selected for each season was based on several
455 tests, with different number of factors and different α -values, taking into account the
456 correlations with external tracers (including nitrate, sulfate, BC and ozone), the daily
457 patterns of each factor, and the residuals. As a result, a solution of 3 factors was
458 selected for each season. In summer, a hydrocarbon-like OA (HOA), a semi-volatile
459 oxygenated OA (SV-OOA) and a low-volatile oxygenated OA (LV-OOA) (Fig.S6) were
460 resolved. The HOA factor was constrained using an average HOA factor from different
461 datasets (Ng et al., 2011b), with an α -value of 0.1. The SV-OOA was characterized by
462 a high 43-to-44 ratio, and the LV-OOA was defined by having a dominant peak at m/z
463 44. In winter the 3 factors identified were: hydrocarbon-like OA (HOA), biomass burning
464 OA (BBOA) and oxygenated OA (OOA) (Fig.S6). The HOA and the BBOA factors were
465 constrained based on the profiles from different datasets (Ng et al., 2011b), with an α -
466 value of 0.1 in both factors, and including BC as an additional variable to the ME-2
467 analysis. The OOA was characterized by a 43-to-44 ratio between those found for the
468 LV-OOA and the SV-OOA in summer, and by having a dominant peak at m/z 44. This
469 high signal of m/z 44 in the winter OOA indicates a high degree of oxidation, and
470 therefore a dominant aged character during winter. A solution with 4 factors in winter
471 was investigated in order to split the OOA into SV-OOA and LV-OOA, but the resulting
472 profiles did not represent two different OOA types, and the time series showed that one
473 of the factors was mainly representing noise. The HOA profiles obtained for the
474 summer and winter periods were similar and showed similar deviations from the Ng et

475 al. (2011b) spectrum (Fig.S7), since they were constrained with the same anchor HOA
476 profile.

477 On average, LV-OOA dominated the OA fraction in summer contributing 64%,
478 followed by SV-OOA (26%) and HOA (10%) (Fig. 8), whereas in winter OOA accounted
479 for 71%, BBOA contributed 24%, and HOA contribution decreased to 5% (Fig. 9). The
480 high contribution of OOA components confirms the initial hypothesis of MSC organic
481 components being mostly secondary in their origin, and it is in agreement with what
482 was found in other remote sites (Freney et al., 2011; Raatikainen et al., 2010).
483 Furthermore, the origin of OA has been recently investigated in the Mediterranean
484 forested area of Montseny, and it has been found that SOA accounted for 91%
485 (Minguillón et al., 2011). The low contribution of primary organic components at MSC is
486 in agreement with the location, since the primary organic emissions are mixed and
487 oxidized during their transport from industrial and urban areas to the remote site of
488 MSC.

489 The diurnal cycles of OA components were studied as a function of air mass
490 origin (Fig. 8 and Fig. 9). A clear daily pattern of OA components was found regardless
491 of the air mass origin, except for Atlantic advections in winter. In summer, the
492 maximum concentrations of LV-OOA and HOA were measured between 12:00 and
493 13:00 UTC, whereas those of SV-OOA were observed between 11:00 and 12:00 UTC.
494 The LV-OOA has been generally associated with highly oxidized, aged, and long-
495 range-transported aerosol particles (Lanz et al., 2010). Conversely, the SV-OOA has
496 been described as the less oxygenated and semi-volatile fraction of OOA (Ng et al.,
497 2011a) and therefore it has been mostly attributed to SOA formation from more local
498 emissions (Jimenez et al., 2009). For this reason, the LV-OOA and HOA hourly
499 variations are more influenced by long-range transport than those of SV-OOA, which
500 are strongly influenced by local/regional processes. In winter, the maximum
501 concentrations of the OA components were observed simultaneously around 14:00
502 UTC. The different daily patterns between seasons can be attributed to the higher
503 production of SOA in summer as opposed to winter, when the maximum daily
504 concentrations are reached later driven by the mountain breezes.

505 **4 Conclusions**

506 This work interprets the real-time variation of inorganic and organic submicron
507 components during 10 months (July 2011 - April 2012) at a high altitude site in
508 southern Europe (Montsec, 1570 m a.s.l.). The aerosol chemical composition was
509 obtained with an ACSM, and co-located on-line and off-line PM₁ measurements were
510 also carried out. The average concentration of the ACSM plus BC mass during this

511 study was $4.9 \mu\text{g m}^{-3}$, and on average OA was the foremost PM_{10} constituent (50%),
512 followed by sulfate (20%), nitrate (14%), ammonium (12%), BC (4%) and chloride (1%).
513 Discrepancies of OA determined by ACSM with co-located measurements pointed to
514 an overestimation by the ACSM probably caused by the use of the default RIE for OA,
515 which could be lower than the actual one. Further research is needed to better address
516 this issue.

517 The seasonal variation of PM_{10} mass and chemical components concentrations
518 showed similar patterns, with an increase in summer and a decrease in winter, except
519 for nitrate which has high volatility in summer. The seasonal variation was attributed to
520 the evolution of the PBL height throughout the year and to synoptic circulation and
521 meteorological factors. At MSC the higher temperature and solar radiation in summer
522 enhances the convection processes, incrementing the development of the PBL, and
523 augments atmospheric photochemistry, promoting the formation of secondary inorganic
524 and organic aerosols.

525 The diurnal variation of PM_{10} components had no clear diurnal patterns in
526 summer, except for organics. This lack of defined daily patterns was ascribed to the
527 recirculation of air masses that causes the formation of reservoir layers at relatively
528 high altitudes, and to the long-range transport from North Africa. These factors result in
529 a high variability of diurnal cycles even within the same type of episode. Nevertheless,
530 organic concentrations had a marked diurnal cycle regardless of the air mass origin,
531 with maximum concentrations around 12:00 UTC. The OA was dominated by LV-OOA
532 (64%), followed by SV-OOA (26%), and HOA (10%). Hence, the midday increase with
533 respect to average concentrations during the night was attributed to the formation of
534 SOA.

535 In winter under regional conditions, concentrations of all PM_{10} components
536 showed much clearer diurnal patterns than in summer, with a maximum between 14:00
537 and 15:00 UTC. These daily cycles were connected to the fact that MSC is located
538 most of the day within the FT, whereas PBL air masses are only injected upwards after
539 midday. However, when MSC was affected by long-range transport from mainland
540 Europe, less marked daily patterns of PM_{10} components were observed.

541 The OA in winter was also mainly secondary (71%), with contributions from
542 BBOA (24%), and HOA (5%). The hourly variation of these factors showed a clear
543 diurnal pattern regardless of the air mass origin, except for Atlantic advections.

544 To the authors' knowledge, this is one of the first times when real-time
545 submicron aerosol chemical composition is characterized and its variation is interpreted
546 during almost a year in a continental background environment. The results obtained in

547 the present study highlight the importance of the SOA formation processes at such
548 remote site as MSC, which could be the objective of further investigations.

549

550 *Acknowledgements.* This study was supported by the Ministry of Economy and
551 Competitiveness and FEDER funds under the PRISMA (CGL2012-39623-C02-1) and
552 CARIATI (CGL2008-06294/CLI) projects, and by the Generalitat de Catalunya (AGAUR
553 2009 SGR8 and the DGQA). The research received funding from the European Union
554 Seventh Framework Programme (FP7/ 2007-2013) ACTRIS under grant agreement no
555 262254. The authors would like to extend their gratitude to the personnel from the COU
556 and the OAdM. We would also like to express our gratitude to the NOAA Air Resources
557 Laboratory (ARL) for the provision of the HYSPLIT transport and dispersion model, and
558 boundary layer height calculation, used in this publication. DAD and JLJ thank DOE
559 (BER/ASR) DE-SC0011105 and NOAA NA13OAR4310063.

560

561 **References**

562 Aiken, A. C., Decarlo, P. F., Kroll, J. H., Worsnop, D. R., Huffman, J. A., Docherty, K.
563 S., Ulbrich, I. M., Mohr, C., Kimmel, J. R., Sueper, D., Sun, Y., Zhang, Q., Trimborn,
564 A., Northway, M., Ziemann, P. J., Canagaratna, M. R., Onasch, T. B., Alfarra, M.
565 R., Prevot, A. S. H., Dommen, J., Duplissy, J., Metzger, A., Baltensperger, U. and
566 Jimenez, J. L.: O/C and OM/OC ratios of primary, secondary, and ambient organic
567 aerosols with high-resolution time-of-flight aerosol mass spectrometry, *Environ. Sci.*
568 *Technol.*, 42(12), 4478–4485, doi:10.1021/es703009q, 2008.

569 Bessagnet, B., Menut, L., Curci, G., Hodzic, A., Guillaume, B., Liousse, C., Moukhtar,
570 S., Pun, B., Seigneur, C. and Schulz, M.: Regional modeling of carbonaceous
571 aerosols over Europe-focus on secondary organic aerosols, *J. Atmos. Chem.*,
572 61(3), 175–202, doi:10.1007/s10874-009-9129-2, 2008.

573 Budisulistiorini, S. H., Canagaratna, M. R., Croteau, P. L., Baumann, K., Edgerton, E.
574 S., Kollman, M. S., Ng, N. L., Verma, V., Shaw, S. L., Knipping, E. M., Worsnop, D.
575 R., Jayne, J. T., Weber, R. J. and Surratt, J. D.: Intercomparison of an Aerosol
576 Chemical Speciation Monitor (ACSM) with ambient fine aerosol measurements in
577 downtown Atlanta, Georgia, *Atmos. Meas. Tech.*, 7(7), 1929–1941,
578 doi:10.5194/amt-7-1929-2014, 2014.

579 Canagaratna, M. R., Onasch, T. B., Wood, E. C., Herndon, S. C., Jayne, J. T., Cross,
580 E. S., Miake-Lye, R. C., Kolb, C. E. and Worsnop, D. R.: Chemical and
581 microphysical characterization of ambient aerosols with the aerodyne aerosol mass
582 spectrometer, *Wiley Interisci.*, 26(2), 185–222, doi:10.1002/mas.20115, 2007.

583 Canonaco, F., Crippa, M., Slowik, J. G., Baltensperger, U. and Prévôt, A. S. H.: SoFi,
584 an IGOR-based interface for the efficient use of the generalized multilinear engine
585 (ME-2) for the source apportionment: ME-2 application to aerosol mass
586 spectrometer data, *Atmos. Meas. Tech.*, 6(12), 3649–3661, doi:10.5194/amt-6-
587 3649-2013, 2013.

- 588 Carbone, C., Decesari, S., Paglione, M., Giulianelli, L., Rinaldi, M., Marinoni, A.,
589 Cristofanelli, P., Diodato, A., Bonasoni, P., Fuzzi, S. and Facchini, M. C.: 3-year
590 chemical composition of free tropospheric PM₁ at the Mt. Cimone GAW global
591 station – South Europe – 2165 m a.s.l., *Atmos. Environ.*, 87, 218–227,
592 doi:10.1016/j.atmosenv.2014.01.048, 2014.
- 593 Carbone, S., Saarikoski, S., Frey, A., Reyes, F., Reyes, P., Castillo, M., Gramsch, E.,
594 Jayne, J., Worsnop, D. R. and Hillamo, R.: Chemical Characterization of Submicron
595 Aerosol Particles in Santiago de Chile, *Aerosol Air Qual. Res.*, 13, 462–473,
596 doi:10.4209/aaqr.2012.10.0261, 2013.
- 597 CEN: Air quality – Determination of the PM₁₀ fraction of suspended particulate matter.
598 Reference method and field test procedure to demonstrate reference equivalence
599 of measurement methods, EN12341:1999, 1999.
- 600 Chevalier, A., Gheusi, F., Delmas, R., Ordóñez, C., Sarrat, C., Zbinden, R., Thouret,
601 V., Athier, G., and Cousin, J.-M.: Influence of altitude on ozone levels and variability
602 in the lower troposphere: a ground-based study for western Europe over the period
603 2001–2004, *Atmos. Chem. Phys.*, 7, 4311–4326, doi:10.5194/acp-7-4311-2007,
604 2007.
- 605 Cozic, J., Verheggen, B., Weingartner, E., Crosier, J., Bower, K. N., Flynn, M., Coe, H.,
606 Henning, S., Steinbacher, M., Henne, S., Collaud Coen, M., Petzold, A. and
607 Baltensperger, U.: Chemical composition of free tropospheric aerosol for PM₁ and
608 coarse mode at the high alpine site Jungfraujoch, *Atmos. Chem. Phys.*, 8(2), 407–
609 423, doi:10.5194/acp-8-407-2008, 2008.
- 610 Crippa, M., Canonaco, F., Lanz, V. A., Äijälä, M., Allan, J. D., Carbone, S., Capes, G.,
611 Dall’Osto, M., Day, D. A., DeCarlo, P. F., Di Marco, C. F., Ehn, M., Eriksson, A.,
612 Freney, E., Hildebrandt Ruiz, L., Hillamo, R., Jimenez, J.-L., Junninen, H., Kiendler-
613 Scharr, A., Kortelainen, A.-M., Kulmala, M., Mensah, A. A., Mohr, C., Nemitz, E.,
614 O’Dowd, C., Ovadnevaite, J., Pandis, S. N., Petäjä, T., Poulain, L., Saarikoski, S.,
615 Sellegri, K., Swietlicki, E., Tiitta, P., Worsnop, D. R., Baltensperger, U. and Prévôt,
616 A. S. H.: Organic aerosol components derived from 25 AMS datasets across
617 Europe using a newly developed ME-2 based source apportionment strategy,
618 *Atmos. Chem. Phys.*, 14, 6159–6176, doi:10.5194/acp-14-6159-2014, 2014.
- 619 Donahue, N. M., Robinson, A. L., Trump, E. R., Riipinen, I. and Kroll, J. H.: Volatility
620 and Aging of Atmospheric Organic Aerosol, *Top. Curr. Chem.*, 339, 97–144,
621 doi:10.1007/128-2012-355, 2014.
- 622 Elbert, W., Taylor, P. E., Andreae, M. O. and Pöschl, U.: Contribution of fungi to
623 primary biogenic aerosols in the atmosphere: wet and dry discharged spores,
624 carbohydrates, and inorganic ions, *Atmos. Chem. Phys.*, 7(17), 4569–4588,
625 doi:10.5194/acp-7-4569-2007, 2007.
- 626 Freney, E. J., Sellegri, K., Canonaco, F., Boulon, J., Hervo, M., Weigel, R., Pichon, J.
627 M., Colomb, A., Prévôt, A. S. H. and Laj, P.: Seasonal variations in aerosol particle
628 composition at the puy-de-Dôme research station in France, *Atmos. Chem. Phys.*,
629 11(24), 13047–13059, doi:10.5194/acp-11-13047-2011, 2011.
- 630 [Fröhlich, R., Crenn, V., Setyan, a., Belis, C. a., Canonaco, F., Favez, O., Riffault, V.,](#)
631 [Slowik, J. G., Aas, W., Aijälä, M., Alastuey, a., Artiñano, B., Bonnaire, N., Bozzetti,](#)
632 [C., Bressi, M., Carbone, C., Coz, E., Croteau, P. L., Cubison, M. J., Esser-Gietl, J.](#)

- 633 [K., Green, D. C., Gros, V., Heikkinen, L., Herrmann, H., Jayne, J. T., Lunder, C. R.,](#)
634 [Minguillón, M. C., Močnik, G., O'Dowd, C. D., Ovadnevaite, J., Petralia, E., Poulain,](#)
635 [L., Priestman, M., Ripoll, a., Sarda-Estève, R., Wiedensohler, a., Baltensperger, U.,](#)
636 [Sciare, J. and Prévôt, a. S. H.: ACTRIS ACSM intercomparison – Part 2:](#)
637 [Intercomparison of ME-2 organic source apportionment results from 15 individual,](#)
638 [co-located aerosol mass spectrometers, Atmos. Meas. Tech. Discuss., 8, 1559–](#)
639 [1613, doi:10.5194/amtd-8-1559-2015, 2015.](#)
- 640 De Gouw, J. and Jimenez, J. L.: Organic aerosols in the Earth's atmosphere., Environ.
641 Sci. Technol., 43(20), 7614–8, doi:10.1021/es9006004, 2009.
- 642 Hallquist, M., Wenger, J. C., Baltensperger, U., Rudich, Y., Simpson, D., Claeys, M.,
643 Dommen, J., Donahue, N. M., Jenkin, M. E., Jimenez, J. L., Kiendler-Scharr, A.,
644 Maenhaut, W., McFiggans, G., Mentel, T. F., Monod, A., Prévôt, A. S. H., Seinfeld,
645 J. H., Surratt, J. D., Szmigielski, R. and Wildt, J.: The formation , properties and
646 impact of secondary organic aerosol : current and emerging issues, Atmos. Chem.
647 Phys., 9(14), 5155–5236, doi:10.5194/acp-9-5155-2009, 2009.
- 648 Henne, S., Furger, M., Nyeki, S., Steinbacher, M., Neininger, B., de Wekker, S. F. J.,
649 Dommen, J., Spichtinger, N., Stohl, A. and Prévôt, A. S. H.: Quantification of
650 topographic venting of boundary layer air to the free troposphere, Atmos. Chem.
651 Phys., 4(2), 497–509, doi:10.5194/acp-4-497-2004, 2004.
- 652 IPCC 2013 in: Climate Change 2013: The Physical Science Basis (Contribution of
653 Working Group I to the Fifth Assessment Report of the Intergovernmental Panel on
654 Climate Change) edited by: Myhre, G., Shindell, D., Breon, F.-M., Collins, W.,
655 Fuglestad, J., Huang, J., Koch, D., Lamarque, J.-F., Lee, D., Mendoza, B.,
656 Nakajima, T., Robock, A., Stephens, G., Takemura, T., and H, Z. Cambridge Univ.
657 Press, UK and New York, USA, 2013.
- 658 Jimenez, J. L., Canagaratna, M. R., Donahue, N. M., Prevot, A. S. H., Zhang, Q., Kroll,
659 J. H., DeCarlo, P. F., Allan, J. D., Coe, H., Ng, N. L., Aiken, A. C., Docherty, K. S.,
660 Ulbrich, I. M., Grieshop, A. P., Robinson, A. L., Duplissy, J., Smith, J. D., Wilson, K.
661 R., Lanz, V. A., Hueglin, C., Sun, Y. L., Tian, J., Laaksonen, A., Raatikainen, T.,
662 Rautiainen, J., Vaattovaara, P., Ehn, M., Kulmala, M., Tomlinson, J. M., Collins, D.
663 R., Cubison, M. J., Dunlea, E. J., Huffman, J. A., Onasch, T. B., Alfarra, M. R.,
664 Williams, P. I., Bower, K., Kondo, Y., Schneider, J., Drewnick, F., Borrmann, S.,
665 Weimer, S., Demerjian, K., Salcedo, D., Cottrell, L., Griffin, R., Takami, A., Miyoshi,
666 T., Hatakeyama, S., Shimono, A., Sun, J. Y., Zhang, Y. M., Dzepina, K., Kimmel, J.
667 R., Sueper, D., Jayne, J. T., Herndon, S. C., Trimborn, A. M., Williams, L. R.,
668 Wood, E. C., Middlebrook, A. M., Kolb, C. E., Baltensperger, U. and Worsnop, D.
669 R.: Evolution of organic aerosols in the atmosphere., Science, 326(5959), 1525–
670 1529, doi:10.1126/science.1180353, 2009.
- 671 Jimenez, J. L., Jayne, J. T., Shi, Q., Kolb, C. E., Worsnop, D. R., Yourshaw, I.,
672 Seinfeld, J. H., Flagan, R. C., Zhang, X., Smith, K. A., Morris, J. W. and Davidovits,
673 P.: Ambient aerosol sampling using the Aerodyne Aerosol Mass Spectrometer, J.
674 Geophys. Res., 108(D7), 8425, doi:10.1029/2001JD001213, 2003.
- 675 Jorba, O., Pandolfi, M., Spada, M., Baldasano, J. M., Pey, J., Alastuey, A., Arnold, D.,
676 Sicard, M., Artiñano, B., Revuelta, M. A. and Querol, X.: Overview of the
677 meteorology and transport patterns during the DAURE field campaign and their
678 impact to PM observations, Atmos. Environ., 77, 607–620,
679 doi:10.1016/j.atmosenv.2013.05.040, 2013.

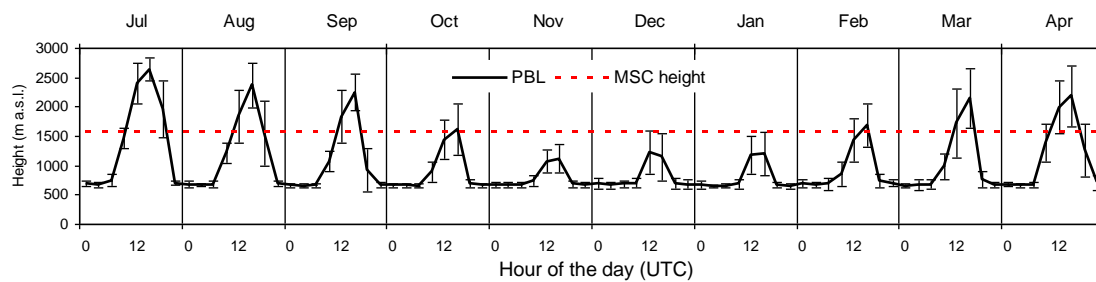
- 680 Kroll, J. H. and Seinfeld, J. H.: Chemistry of secondary organic aerosol: Formation and
681 evolution of low-volatility organics in the atmosphere, *Atmos. Environ.*, 42(16),
682 3593–3624, doi:10.1016/j.atmosenv.2008.01.003, 2008.
- 683 Lang-Yona, N., Rudich, Y., Mentel, T. F., Bohne, A., Buchholz, A., Kiendler-Scharr, A.,
684 Kleist, E., Spindler, C., Tillmann, R. and Wildt, J.: The chemical and microphysical
685 properties of secondary organic aerosols from Holm Oak emissions, *Atmos. Chem.*
686 *Phys.*, 10(15), 7253–7265, doi:10.5194/acp-10-7253-2010, 2010.
- 687 Lanz, V. A., Prévôt, A. S. H., Alfarra, M. R., Weimer, S., Mohr, C., DeCarlo, P. F.,
688 Gianini, M. F. D., Hueglin, C., Schneider, J., Favez, O., D'Anna, B., George, C. and
689 Baltensperger, U.: Characterization of aerosol chemical composition with aerosol
690 mass spectrometry in Central Europe: an overview, *Atmos. Chem. Phys.*, 10(21),
691 10453–10471, doi:10.5194/acp-10-10453-2010, 2010.
- 692 Middlebrook, A. M., Bahreini, R., Jimenez, J. L. and Canagaratna, M. R.: Evaluation of
693 Composition-Dependent Collection Efficiencies for the Aerodyne Aerosol Mass
694 Spectrometer using Field Data, *Aerosol Sci. Technol.*, 46(3), 258–271,
695 doi:10.1080/02786826.2011.620041, 2012.
- 696 Millan, M. M., Salvador, R., Mantilla, E. and Kallos, G.: Photooxidant dynamics in the
697 Mediterranean basin in summer: Results from European research projects, *J.*
698 *Geophys. Res.*, 102, 8811–8823, 1997.
- 699 Minguillón, M. C., Perron, N., Querol, X., Szidat, S., Fahrni, S. M., Alastuey, A.,
700 Jimenez, J. L., Mohr, C., Ortega, A. M., Day, D. A., Lanz, V. A., Wacker, L., Reche,
701 C., Cusack, M., Amato, F., Kiss, G., Hoffer, A., Decesari, S., Moretti, F., Hillamo,
702 R., Teinilä, K., Seco, R., Peñuelas, J., Metzger, A., Schallhart, S., Müller, M.,
703 Hansel, A., Burkhardt, J. F., Baltensperger, U. and Prévôt, A. S. H.: Fossil versus
704 contemporary sources of fine elemental and organic carbonaceous particulate
705 matter during the DAURE campaign in Northeast Spain, *Atmos. Chem. Phys.*,
706 11(8), 23573–23618, doi:10.5194/acp-11-12067-2011, 2011.
- 707 Minguillón, M. C., Ripoll, A., Pérez, N., Prévôt, A. S. H., Canonaco, F., Querol, X. and
708 Alastuey, A.: Chemical characterization of submicron regional background aerosols
709 in the Western Mediterranean using an Aerosol Chemical Speciation Monitor,
710 *Atmos. Chem. Phys. Discuss.*, 15, 965–1000, doi:10.5194/acpd-15-965-2015,
711 2015.
- 712 Müller, T., Henzing, J. S., de Leeuw, G., Wiedensohler, A., Alastuey, A., Angelov, H.,
713 Bizjak, M., Collaud Coen, M., Engström, J. E., Gruening, C., Hillamo, R., Hoffer, A.,
714 Imre, K., Ivanow, P., Jennings, G., Sun, J. Y., Kalivitis, N., Karlsson, H., Komppula,
715 M., Laj, P., Li, S.-M., Lunder, C., Marinoni, A., Martins dos Santos, S., Moerman,
716 M., Nowak, A., Ogren, J. A., Petzold, A., Pichon, J. M., Rodriguez, S., Sharma, S.,
717 Sheridan, P. J., Teinilä, K., Tuch, T., Viana, M., Virkkula, A., Weingartner, E.,
718 Wilhelm, R. and Wang, Y. Q.: Characterization and intercomparison of aerosol
719 absorption photometers: result of two intercomparison workshops, *Atmos. Meas.*
720 *Tech.*, 4(2), 245–268, doi:10.5194/amt-4-245-2011, 2011.
- 721 Ng, N. L., Canagaratna, M. R., Jimenez, J. L., Chhabra, P. S., Seinfeld, J. H. and
722 Worsnop, D. R.: Changes in organic aerosol composition with aging inferred from
723 aerosol mass spectra, *Atmos. Chem. Phys.*, 11(13), 6465–6474, doi:10.5194/acp-
724 11-6465-2011, 2011a.

- 725 Ng, N. L., Canagaratna, M. R., Jimenez, J. L., Zhang, Q., Ulbrich, I. M. and Worsnop,
726 D. R.: Real-Time Methods for Estimating Organic Component Mass Concentrations
727 from Aerosol Mass Spectrometer Data, *Environ. Sci. Technol.*, 45(3), 910–916,
728 doi:10.1021/es102951k, 2011b.
- 729 Ng, N. L., Canagaratna, M. R., Zhang, Q., Jimenez, J. L., Tian, J., Ulbrich, I. M., Kroll,
730 J. H., Docherty, K. S., Chhabra, P. S., Bahreini, R., Murphy, S. M., Seinfeld, J. H.,
731 Hildebrandt, L., Donahue, N. M., DeCarlo, P. F., Lanz, V. A., Prévôt, A. S. H.,
732 Dinar, E., Rudich, Y. and Worsnop, D. R.: Organic aerosol components observed in
733 Northern Hemispheric datasets from Aerosol Mass Spectrometry, *Atmos. Chem.*
734 *Phys.*, 10(10), 4625–4641, doi:10.5194/acp-10-4625-2010, 2010.
- 735 Ng, N. L., Herndon, S. C., Trimborn, A., Canagaratna, M. R., Croteau, P. L., Onasch, T.
736 B., Sueper, D., Worsnop, D. R., Zhang, Q., Sun, Y. L. and Jayne, J. T.: An Aerosol
737 Chemical Speciation Monitor (ACSM) for routine monitoring of the composition and
738 mass concentrations of ambient aerosol, *Aerosol Sci. Technol.*, 45, 780–794,
739 doi:10.1080/02786826.2011.560211, 2011c.
- 740 Paasonen, P., Asmi, A., Petäjä, T., Kajos, M. K., Äijälä, M., Junninen, H., Holst, T.,
741 Abbatt, J. P. D., Arneth, A., Birmili, W., van der Gon, H. D., Hamed, A., Hoffer, A.,
742 Laakso, L., Laaksonen, A., Richard Leaitch, W., Plass-Dülmer, C., Pryor, S. C.,
743 Räisänen, P., Swietlicki, E., Wiedensohler, A., Worsnop, D. R., Kerminen, V.-M.
744 and Kulmala, M.: Warming-induced increase in aerosol number concentration likely
745 to moderate climate change, *Nat. Geosci.*, 6(6), 438–442, doi:10.1038/ngeo1800,
746 2013.
- 747 Paatero, P.: The multilinear engine - a table-driven, least squares program for solving
748 multilinear problems, including the n-way parallel factor analysis model, *J. Comput.*
749 *Graph. Stat.*, 8(4), 854–888, doi:10.2307/1390831, 1999.
- 750 Pandolfi, M., Querol, X., Alastuey, A., Jimenez, J. L., Jorba, O., Day, D., Ortega, A.,
751 Cubison, M. J., Comerón, A., Sicard, M., Mohr, C., Prévôt, A. S. H., Minguillón, M.
752 C., Pey, J., Baldasano, J. M., Burkhardt, J. . F., Seco, R., Peñuelas, J., van Drooge,
753 B. L., Artiñano, B., Di Marco, C., Nemitz, E., Schallhart, S., Metzger, A., Hansel, A.,
754 Lorente, J., Ng, S., Jayne, J. and Szidat, S.: Effects of sources and meteorology on
755 particulate matter in the Western Mediterranean Basin: An overview of the DAURE
756 campaign, *J. Geophys. Res. Atmos.*, 119, 4978–5010, doi:10.1002/2013JD021079,
757 2014a.
- 758 Pandolfi, M., Ripoll, A., Querol, X. and Alastuey, A.: Climatology of aerosol optical
759 properties and black carbon mass absorption cross section at a remote high-
760 altitude site in the western Mediterranean Basin, *Atmos. Chem. Phys.*, 14(12),
761 6443–6460, doi:10.5194/acp-14-6443-2014, 2014b.
- 762 Petit, J.-E., Favez, O., Sciare, J., Crenn, V., Sarda-Estève, R., Bonnaire, N., Močnik,
763 G., Dupont, J.-C., Haefelin, M. and Leoz-Garziandia, E.: Two years of near real-
764 time chemical composition of submicron aerosols in the region of Paris using an
765 Aerosol Chemical Speciation Monitor (ACSm) and a multi-wavelength
766 Aethalometer, *Atmos. Chem. Phys. Discuss.*, 14(17), 24221–24271,
767 doi:10.5194/acpd-14-24221-2014, 2014.
- 768 Petzold, A. and Schönlinner, M.: Multi-angle absorption photometry—a new method for
769 the measurement of aerosol light absorption and atmospheric black carbon, *J.*
770 *Aerosol Sci.*, 35(4), 421–441, doi:10.1016/j.jaerosci.2003.09.005, 2004.

- 771 Petzold, A., Ogren, J. A., Fiebig, M., Laj, P., Li, S.-M., Baltensperger, U., Holzer-Popp,
772 T., Kinne, S., Pappalardo, G., Sugimoto, N., Wehrli, C., Wiedensohler, A. and
773 Zhang, X.-Y.: Recommendations for reporting “black carbon” measurements,
774 *Atmos. Chem. Phys.*, 13(16), 8365–8379, doi:10.5194/acp-13-8365-2013, 2013.
- 775 Pey, J., Pérez, N., Castillo, S., Viana, M., Moreno, T., Pandolfi, M., López-Sebastián, J.
776 M., Alastuey, A. and Querol, X.: Geochemistry of regional background aerosols in
777 the Western Mediterranean, *Atmos. Res.*, 94(3), 422–435,
778 doi:10.1016/j.atmosres.2009.07.001, 2009.
- 779 Pey, J., Querol, X., Alastuey, A., Forastiere, F. and Stafoggia, M.: African dust
780 outbreaks over the Mediterranean Basin during 2001–2011: PM10 concentrations,
781 phenomenology and trends, and its relation with synoptic and mesoscale
782 meteorology, *Atmos. Chem. Phys.*, 13(3), 1395–1410, doi:10.5194/acp-13-1395-
783 2013, 2013.
- 784 Querol, X., Alastuey, A., Lopez-soler, A., Plana, F. and Puigercus, J. A.: Daily evolution
785 of sulphate aerosols in a rural area , northeastern Spain - elucidation of an
786 atmospheric reservoir effect, *Environ. Pollut.*, 105(3), 397–407, doi:10.1016/S0269-
787 7491(99)00037-8, 1999.
- 788 Querol, X., Alastuey, A., Pey, J., Cusack, M., Pérez, N., Mihalopoulos, N., Theodosi,
789 C., Gerasopoulos, E., Kubilay, N. and Koçak, M.: Variability in regional background
790 aerosols within the Mediterranean, *Atmos. Chem. Phys.*, 9(14), 4575–4591,
791 doi:10.5194/acp-9-4575-2009, 2009.
- 792 Raatikainen, T., Vaattovaara, P., Tiitta, P., Miettinen, P., Rautiainen, J., Ehn, M.,
793 Kulmala, M., Laaksonen, A. and Worsnop, D. R.: Physicochemical properties and
794 origin of organic groups detected in boreal forest using an aerosol mass
795 spectrometer, *Atmos. Chem. Phys.*, 10(4), 2063–2077, doi:10.5194/acp-10-2063-
796 2010, 2010.
- 797 Ripoll, A., Minguillón, M. C., Pey, J., Pérez, N., Querol, X. and Alastuey, A.: Joint
798 analysis of continental and regional background environments in the Western
799 Mediterranean: PM1 and PM10 concentrations and composition, *Atmos. Chem.*
800 *Phys.*, 15, 1129–1145, doi:10.5194/acp-15-1129-2015, 2015.
- 801 Ripoll, A., Pey, J., Minguillón, M. C., Pérez, N., Pandolfi, M., Querol, X. and Alastuey,
802 A.: Three years of aerosol mass, black carbon and particle number concentrations
803 at Montsec (southern Pyrenees, 1570 m a.s.l.), *Atmos. Chem. Phys.*, 14(8), 4279–
804 4295, doi:10.5194/acp-14-4279-2014, 2014.
- 805 Robinson, A. L., Donahue, N. M., Shrivastava, M. K., Weitkamp, E. A., Sage, A. M.,
806 Grieshop, A. P., Lane, T. E., Pierce, J. R. and Pandis, S. N.: Rethinking organic
807 aerosols: semivolatile emissions and photochemical aging., *Science*, 315(5816),
808 1259–62, doi:10.1126/science.1133061, 2007.
- 809 Rodríguez, S., Querol, X., Alastuey, A., Kallos, G. and Kakaliagou, O.: Saharan dust
810 contributions to PM10 and TSP levels in Southern and Eastern Spain, *Atmos.*
811 *Environ.*, 35, 2433–2447, doi:10.1016/S1352-2310(00)00496-9, 2001.
- 812 Rodríguez, S., Querol, X., Alastuey, A. and Mantilla, E.: Origin of high summer PM10
813 and TSP concentrations at rural sites in Eastern Spain, *Atmos. Environ.*, 36(19),
814 3101–3112, doi:10.1016/S1352-2310(02)00256-X, 2002.

- 815 Rodríguez, S., Querol, X., Alastuey, A., Viana, M.-M. and Mantilla, E.: Events affecting
816 levels and seasonal evolution of airborne particulate matter concentrations in the
817 Western Mediterranean., *Environ. Sci. Technol.*, 37(2), 216–222,
818 doi:10.1021/es020106p, 2003.
- 819 Salcedo, D., Onasch, T. B., Dzepina, K., Canagaratna, M. R., Zhang, Q., Huffman, J.
820 A., DeCarlo, P. F., Jayne, J. T., Mortimer, P., Worsnop, D. R., Kolb, C. E., Johnson,
821 K. S., Zuberi, B., Marr, L. C., Volkamer, R., Molina, L. T., Molina, M. J., Cardenas,
822 B., Bernabé, R. M., Márquez, C., Gaffney, J. S., Marley, N. A., Laskin, A.,
823 Shutthanandan, V., Xie, Y., Brune, W., Leshner, R., Shirley, T. and Jimenez, J. L.:
824 Characterization of ambient aerosols in Mexico City during the MCMA-2003
825 campaign with Aerosol Mass Spectrometry: results from the CENICA Supersite,
826 *Atmos. Chem. Phys.*, 6(4), 925–946, doi:10.5194/acp-6-925-2006, 2006.
- 827 Schaap, M., Spindler, G., Schulz, M., Acker, K., Maenhaut, W., Berner, A., Wieprecht,
828 W., Streit, N., Müller, K., Brüggemann, E., Chi, X., Putaud, J.-P., Hitznerberger, R.,
829 Puxbaum, H., Baltensperger, U. and ten Brink, H.: Artefacts in the sampling of
830 nitrate studied in the “INTERCOMP” campaigns of EUROTRAC-AEROSOL, *Atmos.*
831 *Environ.*, 38, 6487–6496, doi:10.1016/j.atmosenv.2004.08.026, 2004.
- 832 Seco, R., Peñuelas, J., Filella, I., Llusà, J., Molowny-Horas, R., Schallhart, S.,
833 Metzger, A., Müller, M. and Hansel, A.: Contrasting winter and summer VOC mixing
834 ratios at a forest site in the Western Mediterranean Basin: the effect of local
835 biogenic emissions, *Atmos. Chem. Phys.*, 11(24), 13161–13179, doi:10.5194/acp-
836 11-13161-2011, 2011.
- 837 Sicard, M., Rocadenbosch, F., Reba, M. N. M., Comerón, A., Tomás, S., García-
838 Vízcaíno, D., Batet, O., Barrios, R., Kumar, D. and Baldasano, J. M.: Seasonal
839 variability of aerosol optical properties observed by means of a Raman lidar at an
840 EARLINET site over Northeastern Spain, *Atmos. Chem. Phys.*, 11(1), 175–190,
841 doi:10.5194/acp-11-175-2011, 2011.
- 842 Steinbrecher, R., Smiatek, G., Köble, R., Seufert, G., Theloke, J., Hauff, K., Ciccioli, P.,
843 Vautard, R. and Curci, G.: Intra- and inter-annual variability of VOC emissions from
844 natural and semi-natural vegetation in Europe and neighbouring countries, *Atmos.*
845 *Environ.*, 43(7), 1380–1391, doi:10.1016/j.atmosenv.2008.09.072, 2009.
- 846 Sun, Y., Wang, Z., Dong, H., Yang, T., Li, J., Pan, X., Chen, P. and Jayne, J. T.:
847 Characterization of summer organic and inorganic aerosols in Beijing, China with
848 an Aerosol Chemical Speciation Monitor, *Atmos. Environ.*, 51, 250–259,
849 doi:10.1016/j.atmosenv.2012.01.013, 2012.
- 850 Takahama, S., Schwartz, R. E., Russell, L. M., Macdonald, a. M., Sharma, S. and
851 Leaitch, W. R.: Organic functional groups in aerosol particles from burning and non-
852 burning forest emissions at a high-elevation mountain site, *Atmos. Chem. Phys.*,
853 11(13), 6367–6386, doi:10.5194/acp-11-6367-2011, 2011.
- 854 Tiitta, P., Vakkari, V., Croteau, P., Beukes, J. P., van Zyl, P. G., Josipovic, M., Venter,
855 A. D., Jaars, K., Pienaar, J. J., Ng, N. L., Canagaratna, M. R., Jayne, J. T.,
856 Kerminen, V.-M., Kokkola, H., Kulmala, M., Laaksonen, A., Worsnop, D. R. and
857 Laakso, L.: Chemical composition, main sources and temporal variability of PM1
858 aerosols in southern African grassland, *Atmos. Chem. Phys.*, 14(4), 1909–1927,
859 doi:10.5194/acp-14-1909-2014, 2014.

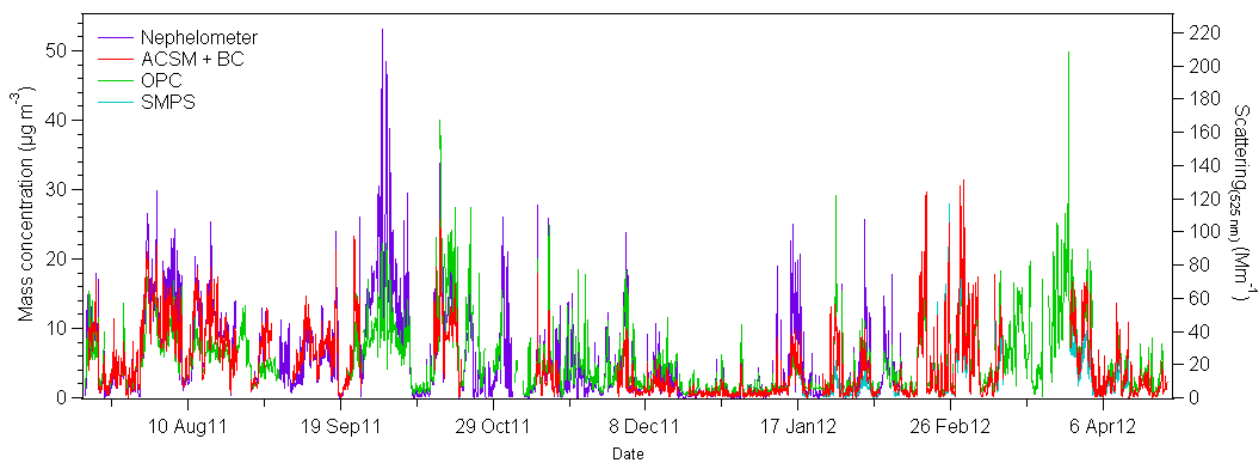
- 860 Tositti, L., Riccio, A., Sandrini, S., Brattich, E., Baldacci, D., Parmeggiani, S.,
861 Cristofanelli, P. and Bonasoni, P.: Short-term climatology of PM₁₀ at a high altitude
862 background station in southern Europe, *Atmos. Environ.*, 65, 142–152,
863 doi:10.1016/j.atmosenv.2012.10.051, 2013.
- 864 Volkamer, R., Jimenez, J. L., San Martini, F., Dzepina, K., Zhang, Q., Salcedo, D.,
865 Molina, L. T., Worsnop, D. R. and Molina, M. J.: Secondary organic aerosol
866 formation from anthropogenic air pollution: Rapid and higher than expected,
867 *Geophys. Res. Lett.*, 33(17), L17811, doi:10.1029/2006GL026899, 2006.
- 868 Zhang, Q., Jimenez, J. L., Canagaratna, M. R., Allan, J. D., Coe, H., Ulbrich, I., Alfarra,
869 M. R., Takami, A., Middlebrook, a. M., Sun, Y. L., Dzepina, K., Dunlea, E.,
870 Docherty, K., DeCarlo, P. F., Salcedo, D., Onasch, T., Jayne, J. T., Miyoshi, T.,
871 Shimono, A., Hatakeyama, S., Takegawa, N., Kondo, Y., Schneider, J., Drewnick,
872 F., Borrmann, S., Weimer, S., Demerjian, K., Williams, P., Bower, K., Bahreini, R.,
873 Cottrell, L., Griffin, R. J., Rautiainen, J., Sun, J. Y., Zhang, Y. M. and Worsnop, D.
874 R.: Ubiquity and dominance of oxygenated species in organic aerosols in
875 anthropogenically-influenced Northern Hemisphere midlatitudes, *Geophys. Res.*
876 *Lett.*, 34(13), L13801, doi:10.1029/2007GL029979, 2007.
- 877 Zhang, Q., Worsnop, D. R., Canagaratna, M. R. and Jimenez, J.-L.: Hydrocarbon-like
878 and oxygenated organic aerosols in Pittsburgh: insights into sources and processes
879 of organic aerosols, *Atmos. Chem. Phys. Discuss.*, 5(5), 8421–8471,
880 doi:10.5194/acpd-5-8421-2005, 2005.
- 881 Zhuang, H., Chan, C. K., Fang, M. and Wexler, A. S.: Size distributions of particulate
882 sulfate , nitrate , and ammonium at a coastal site in Hong Kong, *Atmos. Environ.*,
883 33(6), 843–853, doi:10.1016/S1352-2310(98)00305-7, 1999.



884

885 **Fig. 1 Diurnal variation of the boundary layer height (computed with HYSPLIT model)**
 886 **averaged for each month during the study period at Montsec. Variation bars indicate \pm**
 887 **standard deviation.**

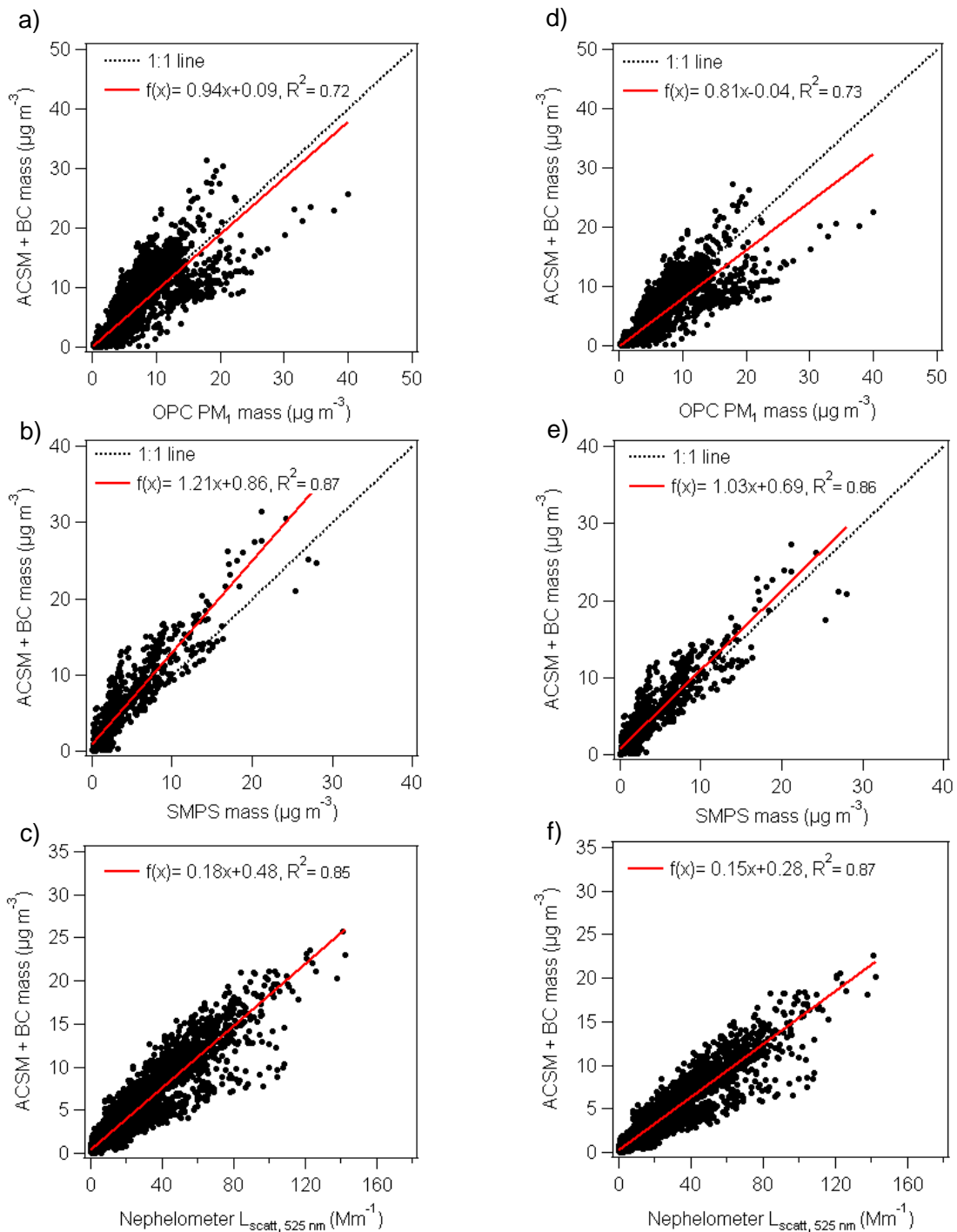
888



889

890 **Fig. 2 Time series of PM₁ total mass from co-located measurements and light scattering**
 891 **at 525 nm.**

892

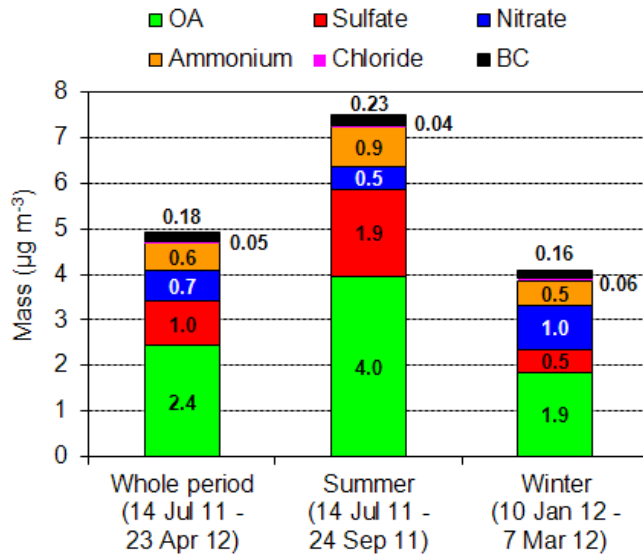


894

895

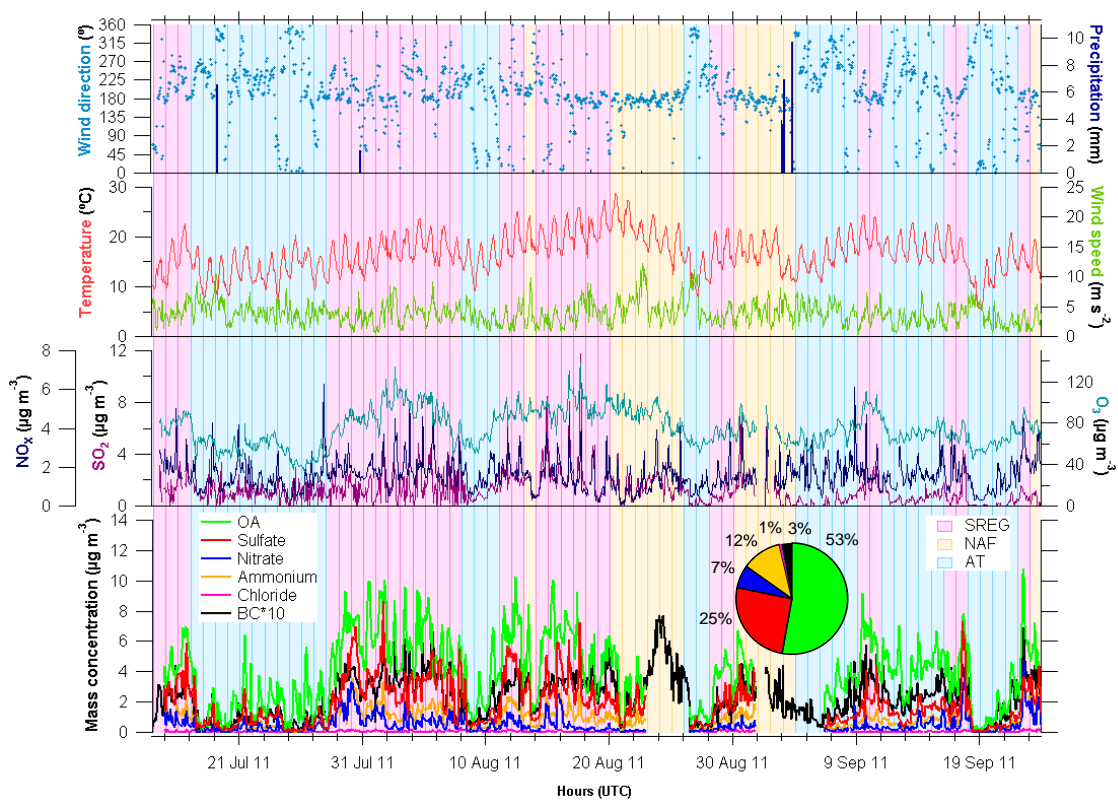
896 **Fig. 3 Top: Scatter plots of ACSM plus BC mass versus PM₁ from (a) OPC and (b) SMPS**
 897 **(winter campaign), and versus light scattering at 525 nm from (c) nephelometer. Bottom:**
 898 **Scatter plots of ACSM plus BC mass after dividing OA by 1.54 versus PM₁ from (d) OPC**
 899 **and (e) SMPS (winter campaign), and versus light scattering at 525 nm from (f)**
 900 **nephelometer. Data points correspond to hourly values. Equations and red lines**
 901 **correspond to linear regression fits.**

902



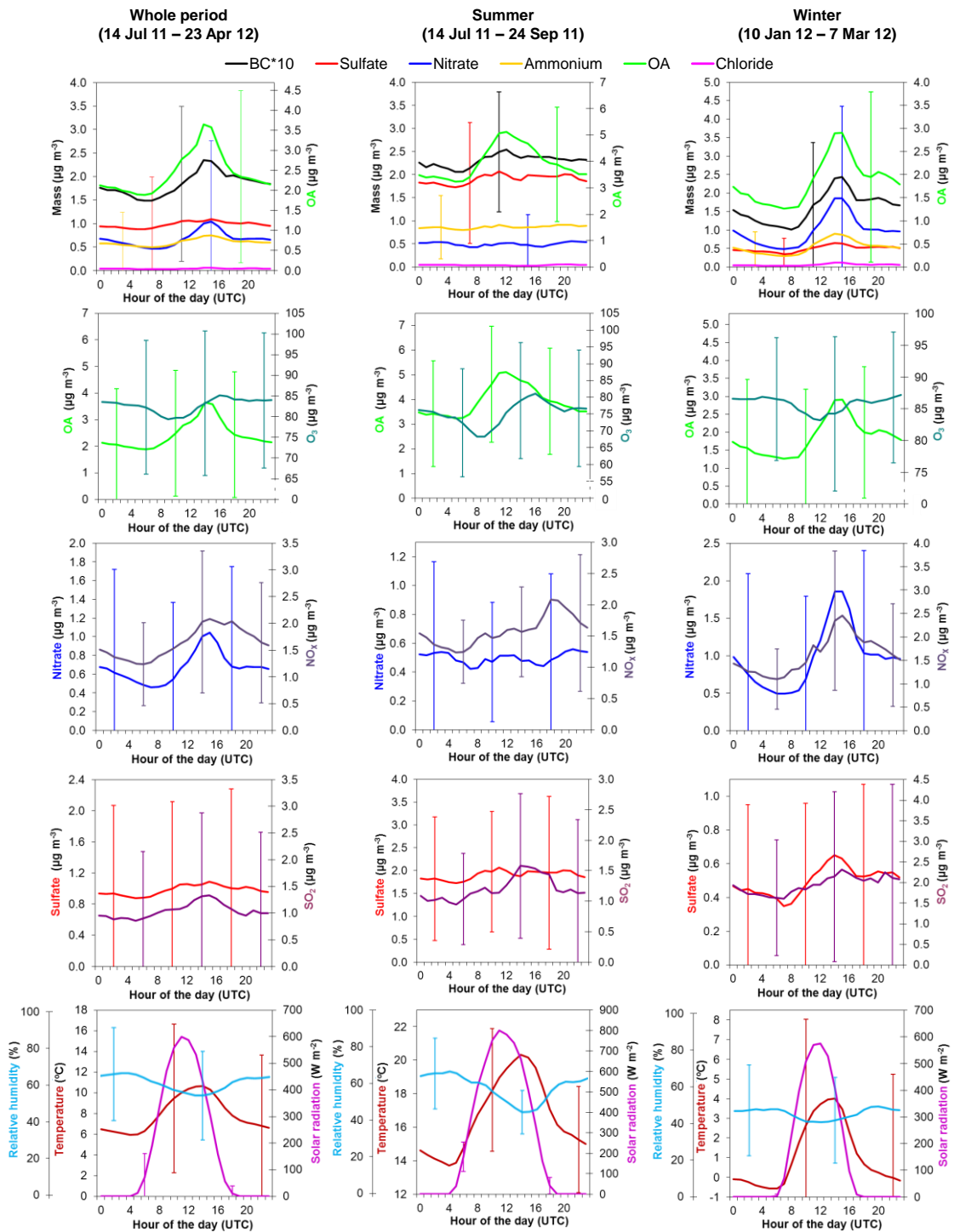
903
904
905
906

Fig. 4 Average concentrations of PM₁ chemical species measured at Montsec during the whole study, in summer and in winter.



907
908
909
910
911
912
913
914

Fig. 5 Time series of wind direction, precipitation, temperature, wind speed, concentrations of nitrogen oxides (NO_x), sulfur dioxide (SO₂), ozone (O₃), and PM₁ chemical species (OA, sulfate, nitrate, ammonium, chloride and black carbon (BC)) in summer (14 Jul 11 – 24 Sep 11). Background colors correspond to daily classification of atmospheric episodes (summer regional (SREG), North African (NAF), and Atlantic (AT)) and the pie chart correspond to the average chemical composition for the summer period.



916

917

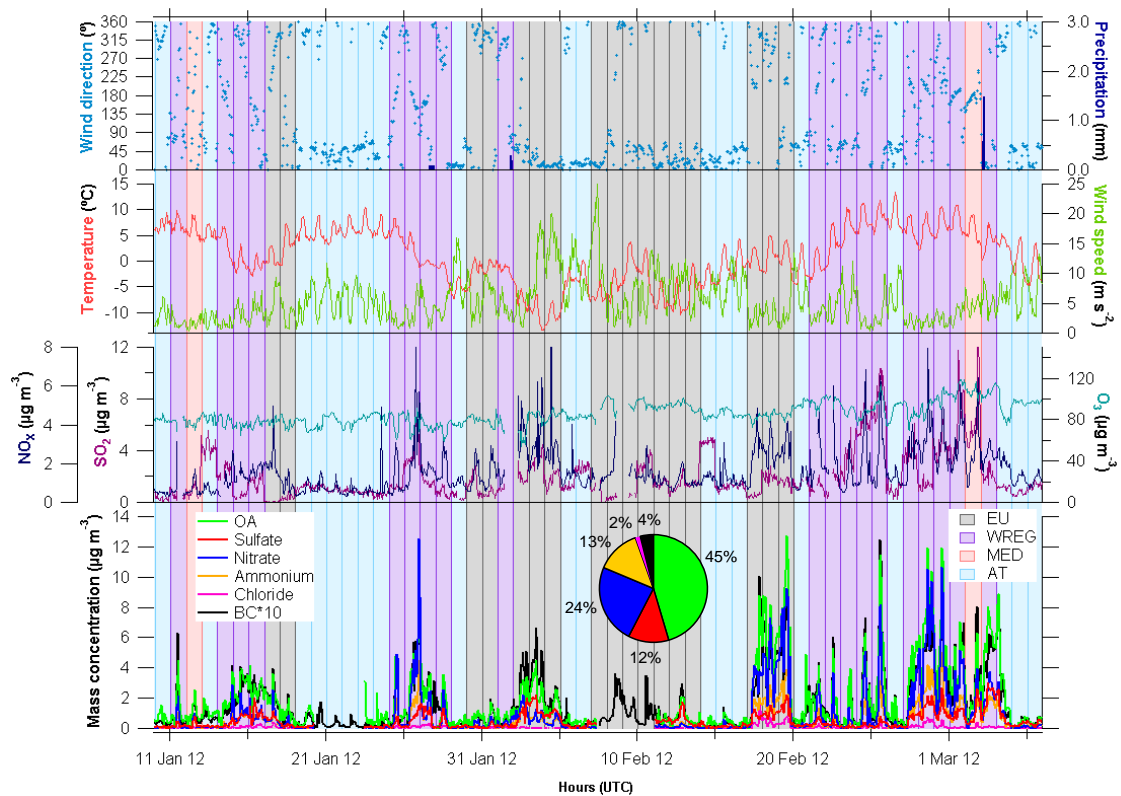
918

919

920

921

Fig. 6 Diurnal cycles of PM₁ chemical species (black carbon (BC), sulfate, nitrate, ammonium, chloride and OA), gaseous pollutants (ozone (O₃), nitrogen oxides (NO_x), and sulfur dioxide (SO₂)), and meteorological parameters (relative humidity, temperature and solar radiation) averaged for the whole period, summer and winter. Variation bars indicate \pm standard deviation.



922

923

924

925

926

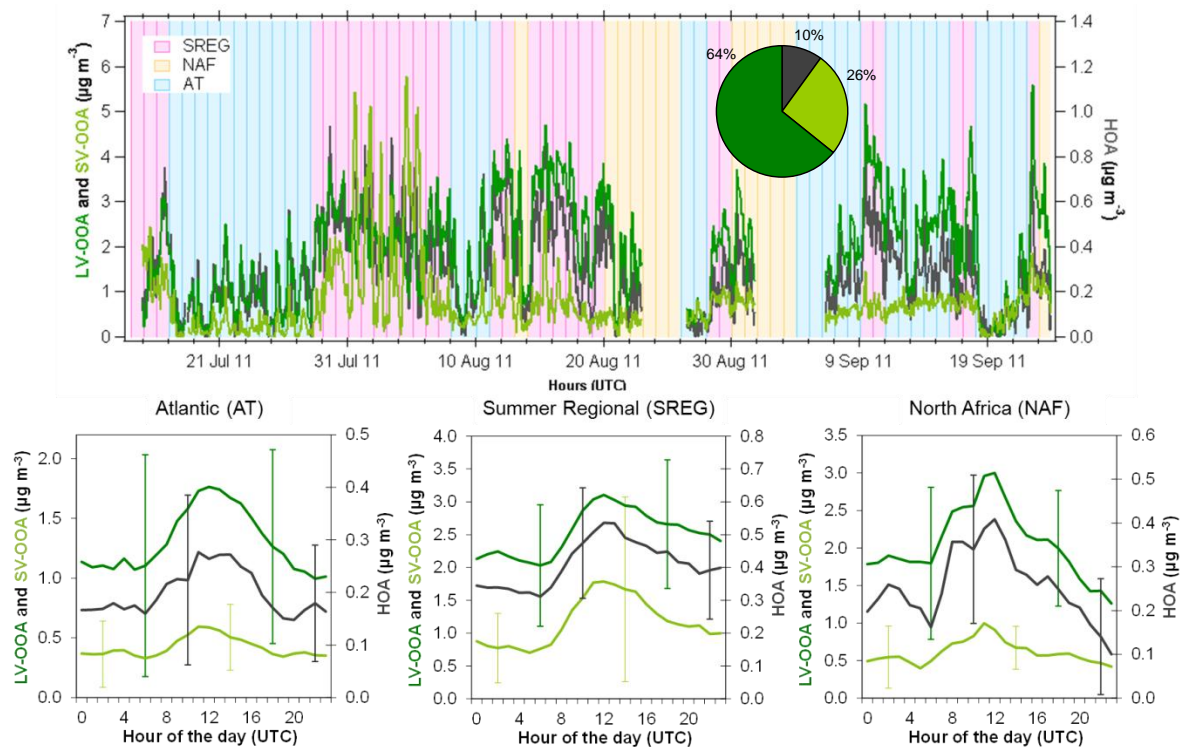
927

928

929

930

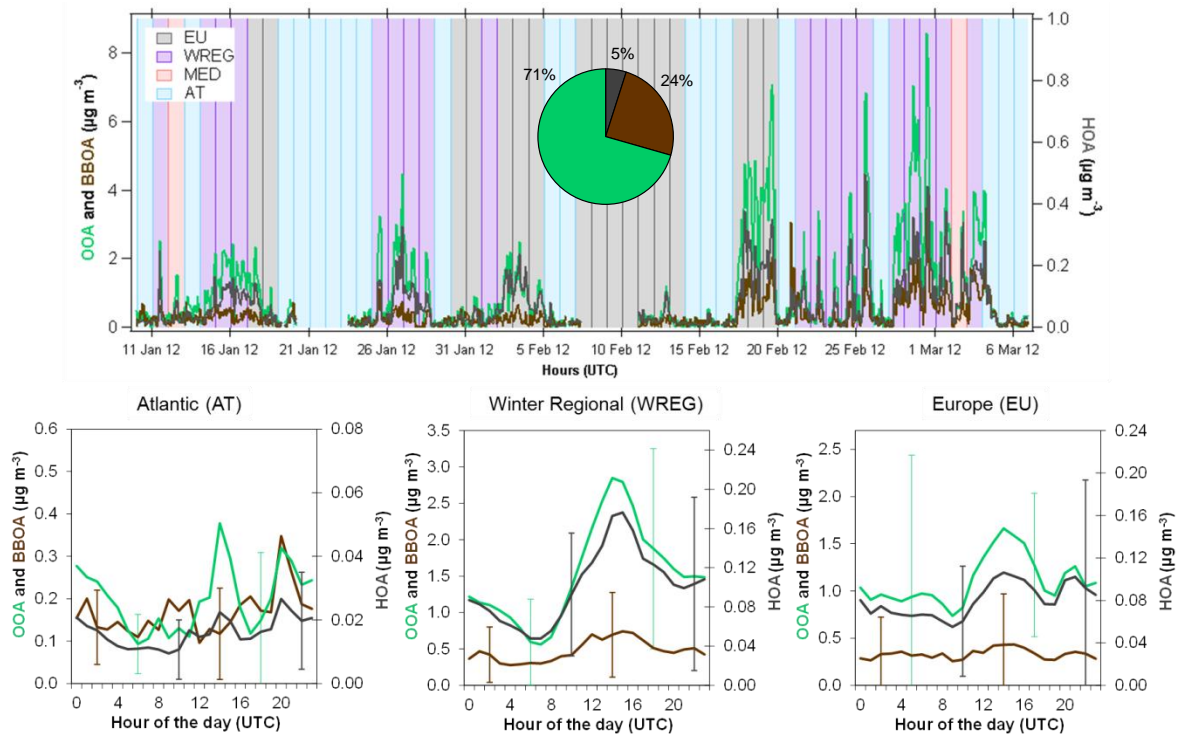
Fig. 7 Time series of wind direction (WD) and speed (WS), temperature (T), precipitation (PP), concentrations of nitrogen oxides (NO_x), sulfur dioxide (SO₂), ozone (O₃), and PM₁ chemical species (organics, sulfate, nitrate, ammonium, chloride and black carbon (BC)) in winter (10 Jan 12 – 7 Mar 12). Background colors correspond to daily classification of atmospheric episodes (European (EU), winter regional (WREG), Mediterranean (MED) and Atlantic (AT)) and the pie chart correspond to the average chemical composition for the winter period.



931

932 **Fig. 8 Top: Time series of organic species (hydrocarbon-like organic aerosol (HOA),**
 933 **semi-volatile oxygenated organic aerosol (SV-OOA) and low-volatility oxygenated**
 934 **organic aerosol (LV-OOA)) concentrations in summer (14 Jul 11 – 24 Sep 11).**
 935 **Background colors correspond to daily classification of atmospheric episodes and the**
 936 **pie chart correspond to the average organic species composition for the summer period.**
 937 **Bottom: Diurnal cycles of organic species concentrations averaged as a function of**
 938 **atmospheric episode for the summer period. Variation bars indicate \pm standard deviation.**

939



941

942 **Fig. 9 Top: Time series of organic species (hydrocarbon-like organic aerosol (HOA),**
 943 **biomass burning organic aerosol (BBOA) and oxygenated organic aerosol (OOA))**
 944 **concentrations in winter (10 Jan 12 – 7 Mar 12). Background colors correspond to daily**
 945 **classification of atmospheric episodes and the pie chart correspond to the average**
 946 **organic species composition for the winter period. Bottom: Diurnal cycles of organic**
 947 **species concentrations averaged as a function of atmospheric episode for the winter**
 948 **period. Variation bars indicate \pm standard deviation.**

949

950

951 **Table 1 Average (25th, 50th, 75th percentiles) concentrations of all chemical components**
 952 **measured at Montsec during the study. Note that the whole period averages include also**
 953 **spring and fall.**

	Whole period ($\mu\text{g m}^{-3}$)	Summer ($\mu\text{g m}^{-3}$)	Winter ($\mu\text{g m}^{-3}$)
Period	14 Jul 11 - 23 Apr 12	14 Jul 11 - 24 Sep 11	10 Jan 12 - 7 Mar 12
Organics	2.4 (0.5, 1.4, 3.8)	4.0 (2.1, 4.0, 5.6)	1.9 (0.4, 1.0, 2.6)
Sulfate	1.0 (0.2, 0.5, 1.4)	1.9 (0.7, 1.6, 2.7)	0.5 (0.1, 0.3, 0.7)
Nitrate	0.7 (0.05, 0.2, 0.7)	0.5 (0.1, 0.3, 0.6)	1.0 (0.05, 0.2, 1.0)
Ammonium	0.6 (0.09, 0.3, 0.9)	0.9 (0.3, 0.8, 1.2)	0.5 (0.06, 0.2, 0.7)
Chloride	0.05 (0.01, 0.02, 0.05)	0.04 (0.01, 0.02, 0.05)	0.1 (0.004, 0.02, 0.1)
BC	0.2 (0.04, 0.1, 0.3)	0.2 (0.1, 0.2, 0.3)	0.2 (0.03, 0.1, 0.2)
Total	4.9 (0.9, 2.8, 7.9)	7.5 (3.4, 7.1, 10.5)	4.1 (0.8, 1.7, 5.6)

954